Monazite-type $SrCrO_4$ under compression

J. Gleissner[1,†], D. Errandonea[1,*], A. Segura[1], J. Pellicer-Porres[1], M. Hakeem[2], J. Proctor[2], S. V. Raju[3], R.S. Kumar[4], Rodríguez-Hernández[5], A. Muñoz[5], and M. Bettinelli[6]

[1]Departamento de Física Aplicada-ICMUV, MALTA Consolider Team, Universidad de Valencia, Edificio de Investigación, C/Dr. Moliner 50, Burjassot, 46100 Valencia, Spain

[2]Joule Physics Laboratory, University of Salford, Manchester M5 4WT, UK

[3]CESMEC, Dept. Mechanical Engineering, Florida International University, Miami, FL, USA

[4]High Pressure Science and Engineering Center, Department of Physics, University of Nevada Las Vegas

[5]Departamento de Física, Instituto de Materiales y Nanotecnología, and MALTA Consolider Team, Universidad de La Laguna, La Laguna, E-38205 Tenerife, Spain

[6]Luminescent Materials Laboratory, Department of Biotechnology, University of Verona and INSTM, UdR Verona, Strada Le Gracie 15, 37134 Verona, Italy

Abstract: We report a high-pressure study of monoclinic monazite-type $SrCrO_4$ up to 26 GPa. In the study we combined x-ray diffraction, Raman and optical-absorption measurements with *ab initio* calculations. We found a pressure-induced structural phase transition in $SrCrO_4$ near 8–9 GPa. Evidence of a second phase transition is found at 10–13 GPa. The crystal structures of the high-pressure phases were assigned to the tetragonal scheelite-type and monoclinic $AgMnO_4$-type structures. Both transitions produce drastic changes in the electronic band gap and phonon spectrum of $SrCrO_4$. We determined the pressure evolution of band gap for the low- and high-pressure phases as well as the frequencies and pressure dependence of the Raman-active modes. In the three phases most Raman modes harden under compression; however the presence of low-frequency modes which gradually soften is also detected. In monazite $SrCrO_4$, the band gap blue shifts under compression and all the Raman phonons harden. The monazite-scheelite transition causes an abrupt decrease of the band gap together with a color change in $SrCrO_4$. Calculations showed a good agreement with experiments and were used to better understand the experimental results. From x-ray diffraction and calculations we determined the pressure dependence of the unit-cell parameters the different phases and their room-temperature equations of state. The results are compared with the high-pressure behavior of other monazites, in particular $PbCrO_4$. A comparison of the high-pressure behavior of the electronic properties of $SrCrO_4$ ($SrWO_4$) and $PbCrO_4$ ($SrCrO_4$) will be also made. Finally, the possible occurrence of a third phase transition is discussed.

† ERASMUS student from Imperial College London, London SW7 2AZ, United Kingdom

* Corresponding author, email: daniel.errandonea@uv.es

I. Introduction

Photocatalytic materials which respond to ultra-violet (UV) and visible (VIS) light can be used in a wide variety of environmental applications [1]. As a consequence of it, they have recently received much attention. In particular, recent progress has been made thanks to the development of chromium-based compounds [1]. Among them, lead chromate ($PbCrO_4$) and strontium chromate ($SrCrO_4$) are the most studied materials due to their unique properties [2 - 5]. The crystal structure of these ternary oxides has been accurately determined [6], being assigned to a monazite-type structure (space group $P2_1/n$, Z = 4). The structural arrangement is based on the nine-fold coordination of the Pb(Sr) cation and the fourfold coordination of the Cr cation. The ambient-pressure lattice vibrations and electronic band structures of $PbCrO_4$ and $SrCrO_4$ have been already studied too [7].

High-pressure (HP) has been shown during the last decade to be an efficient tool for improving the knowledge of the physical properties of ternary oxides [8 – 15]. In particular, monazite-type oxides have been already the subject of HP studies [16 - 19]. These studies have been concentrated mostly in phosphates and vanadates. Among the chromates, monazite-type $PbCrO_4$ is known to have a quite interesting high-pressure behavior [20, 21], undergoing several pressure-induced transitions. These transitions have important consequences in the electronic properties, modifying the electronic band gap from 2.3 eV at ambient pressure to 0.8 eV at 20 GPa [22]. In contrary with $PbCrO_4$ and other monazite-type oxides, to our knowledge no HP studies are available in the literature for $SrCrO_4$.

Here we will report a combined experimental and theoretical study of $SrCrO_4$ under compression. X-ray diffraction (XRD), Raman spectroscopy, and optical-absorption experiments have been carried out up to 26 GPa. *Ab initio* calculations have also been performed. We will report evidence of the existence of at least two phase transitions and propose crystal structures for the HP phases. The transitions have important consequences on the physical properties of $SrCrO_4$, which

will be discussed. The pressure dependence of unit-cell parameters, Raman and infrared (IR) modes, and the electronic band gap will be also reported for the different phases. A comparison of the high-pressure behavior of $SrCrO_4$ and related ternary oxides will be presented too. The reported studies have enabled us to improve the understanding of the HP properties of $SrCrO_4$ and related compounds.

II. Experimental details

$SrCrO_4$ in powder form was prepared by precipitation adding 50 ml of a 1 M $Sr(NO_3)_2$ solution to 50 ml of a 1 M K_2CrO_4 solution. Single crystals were grown using a ternary flux system composed of NaCl, KCl, and CsCl, as described in [23]. The weight composition of the mixture was NaCl (24.8%), KCl (26.4%), CsCl (41.3%) and $SrCrO_4$ (7.5%). The starting reagents were mixed, placed in a platinum crucible with a tight-fitting lid, and kept for 12 h at 620 °C in a horizontal furnace under air atmosphere. The melt was slowly cooled first to 530 °C with a temperature gradient of -1.5 °C/h, then to 450 °C at -2 °C/h, and finally to room temperature at -50 °C/h. The crystals were separated by careful dissolution of the flux in deionized water. Yellow single crystals of about 1 x 1 x 1 mm^3 were obtained. The purity of the synthesized material was confirmed by Energy-dispersive x-ray spectroscopy carried out in transmission-electron microscope (TEM) operated at 200 KeV at the SC-SIE from Universitat de Valencia. It was also verified by powder XRD measurements, using Cu K_α radiation, that the samples were single-phased and presented the monazite-type structure ($P2_1/n$). The unit-cell parameters determined to be a = 7.065(7) Å, b = 7.376(7) Å, c = 6.741(7) Å, and β = 103.1(1)º, in very good agreement with the reported values in the literature [6, 24, 25, 26].

High-pressure powder XDR measurements were performed using a membrane diamond-anvil cell (DAC) and a 4:1 methanol-ethanol mixture as pressure-transmitting medium [27, 28]. The experiments were performed in the angle dispersive geometry with a symmetric-type DAC. A micron-size powder was obtained from the prepared single-crystals and was used in the

experiments. The culet size of diamond anvils was 400 μm and rhenium served as gasket material. The gasket was pre-indented to a thickness of 70 μm and a hole with a diameter of 130 μm was drilled in its center to act as pressure chamber. Special caution was taken in sample loading for avoiding sample bridging between diamond anvils [29]. Pressure was determined using the ruby scale [30]. Experiments were carried out at the beam line 12.2.2 of the Advanced Light Source, Lawrence Berkeley National Laboratory [31] with a MAR345 detector. A monochromatic x-ray wavelength of 0.4949 Å was used for the experiments. The FIT2D software [32] was used to calibrate sample to detector distance and detector tilt and to integrate the two-dimensional diffraction images to standard one dimensional intensity versus 2θ plot. The structural analysis was performed with GSAS and Powdercell software packages [33, 34].

HP Raman spectra were collected in the backscattering geometry using a 632.8 nm He-Ne laser, a single spectrometer (Jobin−Yvon TRH1000), an edge filter and a thermoelectric-cooled multichannel CCD detector (Horiba Synapse). The set-up was calibrated using plasma lines of the He-Ne laser. Two experimental runs were carried out with this set-up. In addition, other two runs were carried out in the backscattering geometry using a 532 nm diode laser. In these experiments, the scattered light was analyzed with a single spectrograph (Shamrock 303i) equipped with an edge filter and an air-cooled multichannel CCD detector (iDus 420). This set-up was calibrated using the Raman lines of Si and diamond. In all the experiments, a laser power of less than 20 mW before the DAC was used to avoid sample heating and the spectral resolution of the system was below 2 cm^{-1}. The experiments were carried out using 10-μm-thick single crystals of $SrCrO_4$ which were loaded either in a symmetric DAC or in a membrane DAC. In both cases we used ultralow fluorescence diamond anvils (300 – 500 μm size) and either inconel or stainless steel gaskets. The gaskets were pre-indented to a thickness of 40-50 μm and a hole of 100-200 μm was used as the pressure chamber. As pressure medium we used either a 16:3:1 methanol-ethanol-water mixture (MEW) or

nitrogen [27]. The four experiments gave similar results. Pressure was determined using the ruby scale [30].

For optical-absorption studies, we used 10-μm-thick parallel face crystals, which were cleaved from the larger single crystals. Measurements in the UV-VS-near-infrared (NIR) range were made with an optical setup that consisted of deuterium and halogen lamps integrated in the DH-2000 light-source from Ocean Optics, fused silica lenses, reflecting optics objectives, and a an Ocean Optics USB2000 UV−VIS−NIR spectrometer [35, 36]. The optical absorption spectra were obtained from the transmittance spectra of the sample, which were recorded using the sample-in, sample-out method [37, 38]. For these experiments we used a membrane DAC equipped by 500 μm culet IIA-type diamonds. The pressure chamber consisted in a 200 μm diameter hole drilled in a 45 μm thick inconel gasket. Ruby fluorescence was used as pressure standard [30] and a mixture of methanol-ethanol-water (16:3:1) was employed as pressure-transmitting medium [27]. Three independent experiments were carried out.

III. Calculations details

Ab initio simulations of $SrCrO_4$ under pressure were performed within the framework of Density-Functional Theory (DFT) [39], as implemented in the Vienna ab Initio Simulation package (VASP) [40]. The pseudopotential with the projector augmented wave scheme (PAW) [41] was employed to describe de atomic species. Due to the presence of oxygen atoms the set of plane waves was developed up to a kinetic energy cut off of 520 eV, in order to obtain accurate results. The exchange-correlation energy was described in the generalized-gradient approximation (GGA) with the Perdew-Burke-Ernzenhof prescription for solids (PBEsol) [42]. To carry out integrations over the Brillouin zone (BZ), dense meshes of Monkhorst-Pack k-special points [43] appropriate to each structure, were used. The convergence achieved in the energy was better than 1 meV per formula unit. For each considered structure, at selected volumes, the lattices parameters and atomic positions, were fully optimized trough the calculation of forces on atoms and the stress tensor. In

the optimized structures, the forces on atoms were less than 0.004 eV/ Å and the deviation of stress tensor components from the diagonal hydrostatic form lower than 0.1 GPa. From the set of energy (E), volume (V), and pressure (P) data, the enthalpy (H) as function of P was obtained and the relative stability between the different phases was analyzed. DFT is a well-tested method which describes accurately the relative phase stability and the properties of semiconductors under pressure [44]. The electronic band structure along high symmetry directions in the Brillouin zone and the density of states were also calculated.

The direct force-constant method [45] was employed to study the lattice vibrations. Lattice dynamic calculations were carried out, under pressure, at the zone center (Γ point) of the BZ. The diagonalization of the dynamical matrix provided the frequency of the Raman and infrared modes. The construction of the dynamical matrix at the Γ point required highly accurate calculations of the forces which appear on the atoms when small displacements from their equilibrium configuration are considered. From the calculations, symmetry and eigenvectors of the vibration modes of the considered structures at the Γ point are also identified. The supercell method was used to obtain the phonon dispersion and the projected phonon density of states.

IV. Results and discussion

Effects of pressure in the crystal structure

From our experiments we found evidence of at least two phase transitions induced by pressure in $SrCrO_4$. These results will be presented below. Since the interpretation of the experiments will be based upon ab initio calculations, we will present first the results of our theoretical study on the structural stability of $SrCrO_4$ at high pressures. In the calculations we have taken into consideration previous results obtained in monazite-type oxides [16, 17, 21, 46] and also candidate HP structures predicted by the packing-efficiency criterion proposed by Bastide [15]. We have studied the relative stability of four candidate HP structures using the calculation method outlined in the previous section. In Fig. 1 we report the difference of enthalpy (taking monazite as reference) of the

structures that we found to be thermodynamically competitive with monazite. At ambient pressure, monazite is the most stable structure of $SrCrO_4$. The calculated structure is reported in Table I where it is compared with experiments previously reported by us [7]. The agreement is excellent. As can be seen in Fig. 1, at 7 GPa a transition from the monoclinic monazite-type structure to a tetragonal scheelite-type structure (space group $I4_1/a$, Z = 4) is found by the calculations. At 12 GPa a subsequent transition to a monoclinic $AgMnO_4$-type structure (space group $P2_1/n$, Z = 4) is obtained in the calculations. Details of the calculated HP crystal structures are given in Table I. The two phase transitions proposed by calculations are in agreement with our experiments and we will report below.

In order to confirm the existence of phase transitions induced by pressure in $SrCrO_4$ we performed room-temperature XRD measurements. A selection of diffraction patterns at different pressures is given in Fig. 2. We found that up to 6.8 GPa the XRD patterns can be Rietveld refined assuming the monazite structure. In the figure we show the results of the experiments carried out at 1.2 GPa and 6.8 GPa together with Rietveld refined profiles and the residuals, which support the identification of the monazite structure. At 1.2 GPa, the goodness-of-fit parameters are: R_P = 4.47%, R_{WP} = 6.76%, and χ^2 = 1.64. Similar figures of merit were obtained at all pressures for the monazite structure; e.g. at 6.8 GPa R_P = 4.94%, R_{WP} = 7.22%, and χ^2 = 1.84. Before discussing the phase transitions induced by pressure in $SrCrO_4$, we would like to mention that when comparing the XRD pattern measured at 6.8 GPa with the one measured at 1.2 GPa, it can be seen that several Bragg peaks split as pressure increases. This is clearly seen in the figure for the (012) and (-112) peaks which are identified. This fact suggests a non isotropic compression of monazite $SrCrO_4$, a point that will be discussed after presenting the evidence of the observed phase transitions.

When increasing the pressure from 6.8 GPa to 9.4 GPa very noticeably changes takes place in the XRD pattern. These changes are consistent with the occurrence of a phase transition at 7.5 GPa as determined from our calculations. The reduction in the number on Bragg reflections is

considerably suggesting a symmetry increase in the crystal structure. In particular, the XRD we measured at 9.4 and 11.2 GPa can be indexed assuming the tetragonal scheelite-type structure. In Fig. 2 we show the results of a Rietveld refinement carried out for the XRD pattern measured at 9.4 GPa. The residuals are small, which indicates that scheelite is a suitable structural model for the crystal structure of the HP phase. The structural information of the scheelite-type phase is given in Table II. The agreement between calculations is good, not only for the unit-cell parameters, but also for the atomic position of the oxygen atoms (The position of Sr and Cr are fixed by the symmetry of the structure). The goodness-of-fit parameters of the refinement shown in Fig. 2 for the scheelite structure are: R_P = 5.74%, R_{WP} = 7.94%, and χ^2 = 2.12.

When increasing the pressure from 11.2 GPa to 13.3 GPa we found evidence of a second phase transition, which agree with the 12 GPa transition pressure found by calculations for the scheelite-$AgMnO_4$-type transition. In particular, the XRD patterns measured from 13.3 GPa up to 18.9 GPa can be properly refined assuming the $AgMnO_4$-type structure. The results of the refinement performed at 13.3 and 16.7 GPa are shown in Fig. 2. The refinements indicate that the $AgMnO_4$-type structure can be assigned to the second HP phase of $SrCrO_4$. The goodness-of-fit parameters of the refinement made for the XRD pattern measured at 13.3 GPa are: R_P = 5.97%, R_{WP} = 8.02%, and χ^2 = 2.19. The obtained unit-cell parameters and atomic positions are given in Table III. The agreement between experiments and calculations is quite good, which give us confidence on the structural assignment made for the second HP phase of $SrCrO_4$. We would like to remark here the fact that the coordination of Cr is not affected in the monazite-scheelite-$AgMnO_4$-type structural sequence, being Cr coordinated by four oxygens forming a regular (or nearly regular) CrO_4 tetrahedron in the three structures.

After a subsequent compression step from 18.9 GPa to 20.4 GPa we observed important changes in the XRD pattern (see Fig. 2). These changes indicate that possible a third phase transition is taking place. Unfortunately, the quality of the XRD pattern measured at 20.4 GPa does

not allow the identification of the crystal structure of the third HP phase, which we will name phase IV. In fact we cannot exclude the phase coexistence of phase IV and the $AgMnO_4$ phase at 20.4 GPa. With the aiming of trying to clarify this last hypothesis we increase the pressure in two steps up to 24 GPa, however, the diffraction peaks become broader that at 20.4 GPa, which preclude any sound structural identification. Thus, from our XRD experiments we can only state that the onset of a third phase transition takes place between 18.9 and 20.4 GPa. This conclusion is supported by our Raman experiments, as we will comment below. The identification of the crystal structure of phase IV remains an open issue for future studies. Before concluding this part of the discussion we would like to mention that upon a rapid decompression from 24 GPa to 0.1 GPa the crystal structure of the low-pressure monazite phase was recovered. This is shown in Fig. 1. There it can be seen that the XRD pattern measured after decompression at 0.1 GPa is quite similar to the one measured at 1.2 GPa during compression.

From the XRD experiments and the calculations we have determined the pressure dependence of the unit-cell parameters. The obtained results are shown in Fig. 3 where the symbols represent the experimental results and the lines are the calculations. We found that the low-pressure phase is slightly more compressible than the two HP phases. This is consistent with the volume reduction associated to each phase transition. In Fig. 3, it can be seen that in both phase transition there is a discontinuity in the volume. At the monazite-scheelite transitition $\Delta V/V$ = -2% according to calculations and -4% according experiments. At the scheelite-$AgMnO_4$ transition $\Delta V/V$ = -4% according to calculations and -2% according experiments. The volume discontinuities are larger than the uncertainty of the volume determination. Thus it can be stated that both transitions are first-order transitions. Regarding the compression of the lattice parameters, we can conclude that the compression in the low-pressure monazite phase is anisotropic, being the *a*-axis the most compressible axis. In addition, it can be seen that the β angle is reduced by compression; approximately 0.2º/GPa. The observed behavior of monazite $SrCrO_4$ is qualitatively similar to that

of other monazites [16 – 20, 47]. In contrast with the low-pressure phase, in the scheelite and $AgMnO_4$ structures the compression is nearly isotropic, being the in the last structure the β angle slightly reduced by compression.

From the pressure dependence of the unit-cell parameters we determined the pressure-volume equation of state (EOS) for the three phases of $SrCrO_4$ and their compressibility tensor. Since we have a few experimental data points for each phase and calculations and experiments agree well we have used the calculations to quantitatively describe the compression of the different phases. We found that for the three phases, the pressure dependence of the volume can be well described by a third-order Birch–Murnaghan EOS [48]. The obtained EOS parameters are summarized in Table IV. In the table V_0 is the unit-cell volume at ambient pressure, B_0 the bulk modulus, and B_0' its pressure derivative. The use of a third-order EOS was based upon an analysis of the dependence of the normalized pressure on the Eulerian strain [49]. The fact that the monazite phase is the one with the smaller bulk modulus is consistent with the fact that it is the most compressible phase of $SrCrO_4$. Regarding the compressibility tensor, in a monoclinic structure this tensor has four independent components β_{11}, β_{22}, β_{33}, and β_{13}. The analytical expressions of them can be found in Ref. [50]. In our monoclinic structures (where *b* is the unique crystallographic axis) β_{22} and β_{33} are the compressibilities of the *b* and *c* axes, respectively. On the other hand β_{11} corresponds to the compressibility in the direction perpendicular to the *b*-*c* plane and β_{13} describes the change of the shape of the plane perpendicular to the unique crystallographic axis. In the case of the tetragonal scheelite structure, given the symmetry of the crystal $\beta_{11} = \beta_{22}$ and $\beta_{13} = 0$. The obtained values for β_{11}, β_{22}, β_{33}, and β_{13} for the three phases are given in Table IV. In the table it can be confirmed that the compression of the low-pressure phase is non isotropic. This is indicated by the fact that β_{33} is more than 20% larger than β_{11} and β_{22}. In contrast in the other two phases the diagonal components of the tensor have values that differs less than 10% among themselves. In the case of the $AgMnO_4$ structure, β_{13} is quite small if compared with the same parameter in the monazite structure. This fact

indicates that the shape of the unit-cell of $AgMnO_4$ is basically not modified by compression. This and the value of the β angle, which is close to 90º, suggest that as a first approximation this HP phase behaves has a quasi-orthorhombic structure, which resembles a distorted-barite structure.

Raman spectroscopy

We will present now Raman spectroscopy evidence on the pressure-driven transitions in $SrCrO_4$. We have previously reported the ambient pressure Raman spectrum of monazite $SrCrO_4$ as well as the mode frequency and assignment of the Raman-active modes [7]. The modes have been identified as internal stretching (high frequency) and bending (intermediate frequency) modes of the CrO_4 tetrahedron and external modes (low frequency), which involve movements of both the Sr^{2+} and CrO_4^{2-} ions [7]. Previously, we have measured at ambient pressure (outside the DAC) thirty of the thirty-six expected modes [7]. Now, we have been able to detect thirty-three modes. The wavenumbers of these modes are given in Table V. In Figures 4 and 5 we show Raman spectra measured at HP using MEW as pressure medium and the 632.8 nm He-Ne laser. To facilitate the mode identification by the readers we have broken the Raman spectra into three regions. They correspond to the external and internal bending and stretching modes, which have very different intensities. The spectra shown in Figure 4 correspond to measurements carried out up to 8.2 GPa. All the Raman spectra shown in this figure resemble the ambient pressure Raman spectrum of monazite $SrCrO_4$. In the HP experiments, we have been able to identify a maximum of twenty-six modes of the monazite phase. The most intense modes are identified by ticks in the figure. The weakest modes observed at ambient pressure (outside the DAC) were not observed at HP because the presence of the diamond anvils increases the background level thereby decreasing the signal-to-noise ratio [51]. We have been able to follow most of the modes up to 8.2 GPa. Up to this pressure the Raman spectra can be undoubtedly identified to the monazite phase. Since not all the modes are equally affected by pressure, we observed the tendency of some of them to merge under compression. We also detected clear evidence of the three phonons crossing over another Raman

mode. Two of the phonon crossovers occur for external modes, and one for internal stretching modes. We found that most of the modes harden under compression. However, we found that two modes have negative pressure coefficients. The frequencies (ω) and pressure coefficients (dω/dP) of the different modes are summarized in Table V where they are compared with our theoretical calculations. The Grüneisen parameters ($\gamma = \frac{B_0}{\omega}\frac{\partial \omega}{\partial P}$), which provide a dimensionless representation of the response to compression, are also included for completeness. The pressure dependence of the Raman frequencies is represented in Figure 6. In the table we have included a column to show the relative difference between experimental and theoretical frequencies R_ω as defined in Ref. 52. For most modes R_ω is smaller than 5% and in many modes is even smaller than 1%, which illustrate the excellent agreement between calculations and experiments. Regarding the pressure dependence of the modes there is a qualitative agreement between calculations and experiments. We observed that the behavior observed in monazite-type $SrCrO_4$ is qualitatively similar to that of isomorphic $PbCrO_4$ [20]. A remarkable feature is the presence of two external modes below 100 cm^{-1} which have negative pressure coefficients. Theory predict the existence of a third mode whose frequency decrease under compression. However, this mode is not detected in our experiments because is expected to be below the low-frequency limit of the Raman set-up. The presence of these modes is apparently a typical feature of monazites since it has been also detected in $PbCrO_4$ [20] and $LaVO_4$ [46]. The presence of such modes might be correlated with a weakening of the restoring force against the corresponding deformation associated to the phonon mode, marking probably the existence of a collective instability that tends to make the crystal structure unstable. This fact is consistent with the finding of a phase transition at relative low pressures as we found in $SrCrO_4$. However, since the wavenumber of the modes with negative pressure coefficients never reaches zero; they are not a classical soft-modes, as those observed in a second-order displacive transition [53, 54]. Another feature we would like to remark is that the tendency of the external modes of

monazite $SrCrO_4$ to have smaller Grüneisen parameters than the internal modes. The same trend has been observed before not only in monazite $PbCrO_4$ [20] but also in barite-type $BaCrO_4$ [55].

When increasing the pressure from 8.2 GPa to 8.9 GPa very important changes take place in the Raman spectrum. In the spectrum measured at 8.9 GPa only eleven modes can be identified. The observed changes indicate the occurrence of a phase transition. The transition pressure is consistent with the monazite-scheelite transition pressure obtained from XRD and calculations. The mode distribution of phonons in the Raman spectrum is very similar to that of most scheelite oxides [56]. The Raman spectrum of the scheelite structure has thirteen Raman-active modes [56]. In our case we detected only eleven. One of the modes not detected usually is very week. The other mode is not detected because of the degeneration of two modes. Confirmation of the assignment of the Raman spectrum measured at 8.9 GPa to the scheelite phase comes from ab initio calculations. In Table VI we report the Raman frequencies determined from experiments and calculations. All frequencies agree within 5% supporting that the measured Raman spectrum can be assigned to the HP scheelite structure. Calculations also provide the mode assignment which is given in the table. A typical feature of the scheelite Raman spectrum is the presence of three strong modes in the high-frequency region, which are indeed present in the spectra we assigned to the scheelite structure. The modes are internal stretching modes of the CrO_4 tetrahedron and are separated by a large phonon gap from the rest of the phonons (see Table VI). When increasing the pressure we observed the scheelite phase, as a single phase, in a sharp pressure range because of the onset of a second phase transition at 9.7 GPa (see discussion below). However, the most intense peaks of the scheelite phase can be detected up to 11.7 GPa. The phonon frequencies as function of pressure are shown in Figure 6. From these results we estimate the pressure coefficient of each phonon. The coefficients are shown in Table VI where they are compared with calculations. The agreement is not as good as for the frequencies, however differences are comparable with the discrepancy observed between theory and calculations for the HP phases of relates oxides [57]. The mode for which the largest discrepancy is observed for the pressure dependence of the frequency is the low frequency B_g

modes at 127 cm^{-1}. In spite of these facts, both methods gave a qualitatively similar picture, suggesting that in scheelite $SrCrO_4$, as it happens in the low-pressure monazite phase, the external modes ($\omega < 375$ cm^{-1}) are the modes with the largest Grüneisen parameters. In addition, as in the monazite phase, in scheelite $SrCrO_4$ there is also a phonon with a negative pressure coefficient. This is a phonon with the lowest frequency (see Table VI). The pressence of a mode with such a behavior is a distinctive feature of scheelite-structure oxides [5].

Aa we commented above, at 9.7 GPa, additional Raman modes appear in the spectra suggesting the onset a second phase transition. We found evidence of the coexistence of the scheelite phase with the new HP phase up to 11.7 GPa. The modes of the new phase gradually become stronger while the modes of scheelite loss intensity. At 12.2 GPa the scheelite modes have completely vanished. The existence of this second transition is in agreement with the conclusions drawn from our XRD experiments and calculations. It is noticeably that the new HP phase has many more Raman modes than scheelite, which is consistent with the scheelite-$AgMnO_4$ transition. From 12.2 GPa to 14.7 GPa we did not observe any qualitative change in the Raman spectrum. We will show below that the calculated Raman frequencies for the $AgMnO_4$ phase agree reasonably well with the modes we identified in the experiments. At 15.7 GPa we observe the appearance of several additional Raman modes and the disappearance of part of the modes of the $AgMnO_4$ phase. We consider these changes have evidenced another phase transition to a phase we named as phase IV. As we mentioned above these transition was detected by XRD at 20.4 GPa and its identification is beyond the scope of this work. We would like to mention here that the same transition was detected when using nitrogen as pressure medium at 19.5 GPa. The differences is the transition pressures for the $AgMnO_4$-phase IV transition can be caused by the use of different pressure media, which have a different hydrostatic pressure limit [27] influencing therefore the transition pressures of compounds like $SrCrO_4$ [59, 60]. Before discussing more in detail the Raman modes of $AgMnO_4$-type $SrCrO_4$, we would like to ad that we observed that phase IV remains stable up to 26 GPa.

From factor group analysis, it can be established that the $AgMnO_4$ structure presents 36 Raman-active phonons (Γ = 18Bg + 18Ag), exactly as the monazite phase has. The expected number of Raman modes is consistent with the changes we observed in the Raman spectra near the scheelite-$AgMnO_4$ transition pressure. The calculated wavenumbers and mode assignment of all Raman-active modes for the $AgMnO_4$-type structure are given in Table VII. We have eighteen low-frequency lattice modes plus eight internal bending modes and eight internal stretching modes of the CrO_4 tetrahedron. In the experiments we have detected also thirty six modes. A correlation can be established between calculated and measured frequencies for the sixteen low-frequency lattice modes. However, the internal modes cannot be fully correlated. In fact, for the intermediate frequency range ($340 < \omega < 450$ cm^{-1}) we have measured only eight modes, whereas calculations predict ten modes. The missing of two modes could be caused by the fact that experiments predicts that two couples of A_g/B_g are very close in frequency. This added two the fact that modes broaden and lost intensity as pressure increase could justify the detection of only eight Raman modes instead of the expected ten modes. In the high-frequency region the opposite behavior is found. Eight modes are predicted by theory while we observed ten modes in the experiments. The two extra modes could be overtones of the low-frequency modes or be induced by a disorder in the crystal structure as previously observed when disorder is induced in related oxides [60, 61]. In summary, in spite of these facts, we can state that calculations and experiments show an qualitative overall agreement on the Raman spectrum of the second HP phase of $SrCrO_4$, indicating that the $AgMnO_4$-type structure we determined from XRD and calculations gives a good model to explain the Raman spectrum of the second HP phase. Regarding the pressure dependence of the Raman modes, the agreement between experiments and calculations is good. Even better than for the scheelite phase. The main difference between the $AgMnO_4$ and the other two phases is that in the $AgMnO_4$ phase the external and internal modes have similar Grüneisen parameters. Another fact to remark on the $AgMnO_4$ phase is that it has two phonons with negative pressure coefficients, which are the two lowest frequency modes.

Optical absorption and band structure

Figure 7 shows a selection of optical-absorption spectra measured at different pressures. From our measurements we determined that the $SrCrO_4$ is an indirect band-gap material with band-gap energy (Eg) of 2.45(5) eV. Our band-structure calculations confirms that $SrCrO_4$ has an indirect band gap giving Eg = 2.67 eV. The agreement between calculations and experiments is good; being Eg overestimated a 9% by theory. As pressure increase we observed that the absorption spectrum shifts towards higher energy, becoming the orange color of the $SrCrO_4$ crystal more yellowish, which suggests an increase of Eg. At 8.3 GPa we observed an abrupt shift of the absorption spectrum towards low energies. At this pressure the crystal of $SrCrO_4$ changes it color becoming orange-red. This abrupt change in the optical properties correlates well with the occurrence of the monazite-scheelite transition. Upon further compression, there is a blue-shift of the absorption spectrum of $SrCrO_4$. From the optical-absorption measurements we determined the pressure dependence of Eg up to 15 GPa. The results are summarized in Figure 8. For the low-pressure phase, we found a gradual increase of Eg under compression. Assuming there is a linear dependence relation between Eg and pressure we determined dEg/dP = 17(5) meV/GPa. This pressure coefficient contrast with pressure coefficient determined for the band gap of monazite $PbCrO_4$ (-46 meV/GPa) [22]. Note than the same differences are found when comparing the pressure effect on the band gap of $SrWO_4$ (dEg/dP = 3.7 meV/GPa) and $PbWO_4$ (dEg/dP = -61 meV/GPa) [35]. An explanation to the observed difference comes from band structure calculations. Our calculations indicate that in both compounds, the upper part of the valence band is dominated by O 2p states. On the contrary, the lower part of the conduction band is composed primarily of electronic states associated with the Cr 3d and O 2p states. On the other hand, in $SrCrO_4$ the Sr states are completely empty near the Fermi level. Thus, they do not have any influence on the bandgap energy. However, in $PbCrO_4$, there is a contribution of Pb 6s electrons to the top of the valence band and of Pb 6p states to the bottom of the conduction band. As a consequence, Eg is smaller in $PbCrO_4$ (2.25 eV) than in $SrCrO_4$ (2.45 eV). Another consequence is the different

behavior of Eg with pressure in both compounds. From our calculations, we found that under compression in $SrCrO_4$ Cr 3d states moves faster towards higher energies that O 2p states, leading the small opening of the band gap we observed in the experiments. In contrast, in $PbCrO_4$, the top of the valence band shifts toward high energies faster than the bottom of the conduction band. This is a consequence that under compression the separation between Pb bonding and anti-bonding states is enlarged. This fact enhances the displacement towards higher energies of the top of the valence band, but reduces the displacement of the bottom of the conduction band.

At 8.3 GPa we observed an abrupt decrease of 0.2 eV in Eg (see Figure 8). This pressure corresponds to the monazite-scheelite transition we described above. We carried out band-structure calculations for scheelite-type $SrCrO_4$. Calculations indicate that in the scheelite structure $SrCrO_4$ is a direct band-gap material with Eg = 2.25 eV (at 8.3 GPa) with the band gap located at the Γ point of the Brilloun zone. This value of Eg is 6% smaller than the experimental value determined for the scheelite phase; Eg = 2.40(5) eV. The band-gap collapse determined from calculations is 0.4 eV. Summing up, the changes observed in the optical properties of $SrCrO_4$ at 8.3 GPa are consistent with the structural sequence found in our structural and vibrational studies. Upon further compression we observed that in the scheelite phase Eg linearly increases with pressure, being dEg/dP = 16(5) meV/GPa, nearly identical than in the low-pressure phase. This result is consistent with the fact that in both structures the valence and conduction bands near the band gap are dominated by molecular orbitals associated with the CrO_4^{-2} ions, and the fact that the CrO_4 tetrahedron undergoes a similar compression in both structures.

At 10.2 GPa we found a change in the pressure dependence of Eg. This change is consistent with the existence of the second phase transition we proposed based upon our structural and vibrational studies. For the second HP phase we determined dEg/dP = 4(2) meV/GPa; which indicates that Eg is less sentive to pressure in the $AgMnO_4$-type phase. The decrease of dEg/dP in this phase is consistent with the fact that this is the less compressible structure among the three

structures here reported for $SrCrO_4$. For the second HP phase we experimentally determined Eg = 2.46(5) eV at 14.5 GPa. Our calculations for the $AgMnO_4$-type phase give Eg = 2.45 eV; i.e. the agreement is excellent. According with our calculation in this phase $SrCrO_4$ is an indirect band gap material, with the top of the valence band at the Y point of the Brillouin zone and the bottom of the conduction band at the Γ point.

V. Summary

We have performed HP XRD, Raman, and optical-absorption measurements as well as ab initio calculations on $SrCrO_4$. Changes in the structural, lattice dynamics, and optical properties indicate the occurrence of at least two phase transitions. *Ab inito* calculations confirm the experimental findings and help to understand them. We have assigned a scheelite-type and a $AgMnO_4$-type structure to the two new polymorphs found in $SrCrO_4$. The pressure dependence of unit-cell parameters, Raman modes, and band-gap energy is reported for the low-pressure monazite phase and the two HP phases of $SrCrO_4$. An assignment for the Raman modes is proposed based upon calculations. The reported results contribute to improve the understandings of the effects of pressure in the physical properties of ternary oxides. A comparison with the behavior of the band gap of $SrCrO_4$ and $PbCrO_4$ is presented and an explanation to their different HP behavior is proposed.

ACKNOWLEDGMENTS

Acknowledgments

This work has been done under financial support from Spanish MINECO under projects MAT2013-46649-C4-1/3-P and MAT2015-71070-REDC. Supercomputer time has been provided by the Red Española de Supercomputación (RES) and the MALTA cluster. The authors thank the SCSIE from Universitat de Valencia the technical support.

References

[1] L. K. Bharat, L. S. Reddy, and J. S. Yu, Materials Letters **144**, 85 (2015) and reference therein.

[2] J. Yin, Z. Zou, and J. Ye, Chem Phys Lett **378**, 24 (2003).

[3] M. U. Belyi, S. G. Nedel'ko, and O. V. Chukova, J. Appl. Spectrosc. **62**, 604 (1995).

[4] P. Chen, Q. S. Wu, Y. P. Ding, and P. S. Yuan, Bull. Mater. Sci. **31**, 603 (2008).

[5] G. A. M. Dalhoeven and G. Blasse, Chem. Phys. Lett. **76**, 27 (1980).

[6] H. Effenberger and F. Pertlik, Zeitschrift fur Kristallographie **176**, 75 (1986).

[7] D. Errandonea, A. Muñoz, P. Rodríguez-Hernández, J. Proctor, F. Sapiña, and M. Bettinelli, Inorg. Chem. **54**, 7524 (2015).

[8] D. Errandonea, C. Popescu, A. B. Garg, P. Botella, D. Martinez-Garcıa, J. Pellicer-Porres, P. Rodrıguez-Hernandez, A. Muñoz, V. Cuenca-Gotor, and J. A. Sans, Phys. Rev. B **93**, 035204 (2016).

[9] J. Ruiz-Fuertes, S. Lopez-Moreno, J. Lopez-Solano, D. Errandonea, A. Segura, R. Lacomba-Perales, A. Muñoz, S. Radescu, P. Rodrıguez-Hernandez, M. Gospodinov, L. L. Nagornaya, and C. Y. Tu, Phys. Rev. B **86**, 125202 (2012).

[10] J. Ruiz-Fuertes, A. Segura, F. Rodríguez, D. Errandonea, and M. N. Sanz-Ortiz, Phys. Rev. Lett. **108**, 166402 (2012).

[11] P. Goel, M. K. Gupta, R. Mittal, S. Rols, S. N. Achary, A. K. Tyagi, and S. L. Chaplot, Phys. Rev. B **91**, 094304 (2015).

[12] D. Errandonea, Cryst. Res. Technol. **50**, 729 (2015).

[13] D. Errandonea, L. Gracia, R. Lacomba-Perales, A. Polian, and J. C. Chervin, J. Appl. Phys. **113**, 123510 (2013).

[14] M. N. Coelho, P. T. C. Freire, M. Maczka, C. Luz-Lima, G. D. Saraiva, W. Paraguassu, A. G. Souza Filho, N. D. P. S. Pizani, Vibrat. Spectr. **68**, 34 (2013).

[15] D. Errandonea and F. J. Manjon, Prog. Mater. Sci. **53**, 711 (2008).

[16] R. Lacomba-Perales, D. Errandonea, Y. Meng, and M. Bettinelli, Phys. Rev. B **81**, 064113

(2010).

[17] D. Errandonea, C. Popescu, S.N. Achary, A. K. Tyagi, and M. Bettinelli, Mater. Res. Bull. **50**, 279 (2014).

[18] D. Errandonea, O. Gomis, D. Santamaria-Perez, B. Garcia-Domene, A. Muñoz, P. Rodriguez-Hernandez, S. N. Achary, A. K. Tyagi, and C. Popescu, J. Appl. Phys. **117**, 105902 (2015).

[19] T. Huang, J. S. Lee, J. Kung, and C. M. Lin, Solid State Commun. 150, 1845 (2010).

[20] E. Bandiello, D. Errandonea, D. Martinez-Garcia, D. Santamaria-Perez, and F. J. Manjon, Phys. Rev. B **85**, 024108 (2012).

[21] D. Errandonea and R. S. Kumar, Mater. Res. Bull. **60**, 206 (2014).

[22] D. Errandonea, E. Bandiello, A. Segura, J. J. Hamlin, M. B. Maple, P. Rodriguez-Hernandez, and A. J. Alloys Compd. **587**, 14 (2014).

[23] R. P. Schenker, T. C. Brunold, H. U. Güdel, Inorg. Chem. **37**, 918 (1998).

[24] C. W. F. T. Pistorius and M. C. Pistorius, Zeitschrift fur Kristallographie **117**, 259 (1962).

[25] J. Yin, Z. Zou, amd J. Ye, Chem. Phys. Letters **378**, 24 (2003).

[26] P. Pahri and V. Manivannan, J. Alloys Compd. **469**, 558 (2009).

[27] S. Klotz, J. C. Chervin, P. Munsch, and G. Le Marchand, J. Phys. D: Appl. Phys. **42**, 075413 (2009).

[28] D. Errandonea, Y. Meng, M. Somayazulu, and D. Häusermann, Physica B **355**, 116 (2005).

[29] D. Errandonea, A. Muñoz, and J. Gonzalez-Platas, J. Appl. Phys. **115**, 216101 (2014).

[30] H. K. Mao, J. Xu, and P. M. Bell, J. Geophys. Res. **91**, 4673 (1986).

[31] M. Kunz, A. A. MacDowell, W. A. Caldwell, D. Cambie, R. S. Celestre, E. E. Domning, R. M. Duarte, A. E.

Gleason, J. M. Glossinger, N. Kelez, D. W. Plate, T. Yu, J. M. Zaug, H. A. Padmore, R. Jeanloz, A. P. Alivisatos and S. M. Clark, J. Synchrotron Rad.**12**, 650 (2015).

[32] A. Hammersley, S. O. Svensson, M. Hanfland, A. M. Fitch, and D. H¨aussermann, High. Press. Res. **14**, 235 (1996).

[33] A.C. Larson, R.B. von Dreele, Los Alamos National Laboratory Report No. 86-748, 2004 (unpublished).

[34] W. Kraus, G. Nolze, J. Appl. Crystallogr. **29** (1996) 301.

[35] R. Lacomba-Perales, D. Errandonea, A. Segura, J. Ruiz-Fuertes, P. Rodriguez-Hernandez, S. Radescu, J. Lopez-Solano, and A. Mujica, J. Appl. Phys. **110**, 043703 (2011).

[36] A. Segura, J. A. Sans, D. Errandonea, D. Martinez-Garcia, and V. Fages, Appl. Phys. Lett. **88**, 011910 (2006).

[37] V. Panchal, D. Errandonea, A. Segura, P. Rodriguez-Hernandez, A. Muñoz, S. Lopez-Moreno, and M. Bettinelli, J. Appl. Phys. **110**, 043723 (2011).

[38] D. Errandonea, D. Martinez-Garcia, R. Lacomba-Perales, J. Ruiz-Fuertes, and A. Segura, Appl. Phys. Lett. **89**, 091913 (2006).

[39] P. Hohenberg and W. Kohn, Phys. Rev. **136**, B864 (1964).

[40] G. Kresse and J. Hafner, Phys. Rev. B **47**, 558 (1993).

[41] G. Kresse and D. Joubert, Phys. Rev. B **59**, 1758 (1999).

[42] J. P. Perdew, A. Ruzsinszky, G. I. Csonka, O. A. Vydrow, G. E. Scuseria, L. A. Constantin, Z. Zhou, and K. Burke, Phys. Rev. Lett. **100**, 136406 (2008).

[43] H. J. Monkhorst and J. D. Pack, Phys. Rev. B **13**, 5188 (1976).

[44] A. Mujica, A. Rubio, A. Muñoz, and R. J. Needs, Rev. Mod. Phys. **79**, 863 (2003).

[45] K. Parlinski, Computer Code PHONON. See: http://wolf.ifj.edu.pl/phonon

[46] D. Errandonea, J. Pellicer-Porres, D. Martínez-García, J. Ruiz-Fuertes, A. Friedrich, W. Morgenroth, C. Popescu, P. Rodríguez-Hernández, A. Muñoz, and M. Bettinelli, submitted to Phys. Rev. B (2016) arXiv:1603.07095.

[47] D. Errandonea, R. S. Kumar, S. N. Achary, and A. K. Tyagi, Phys. Rev. B **84**, 224121 (2011).

[48] F. Birch, J. Geophys. Res. **83**, 1257 (1978).

[49] R.J. Angel, Rev. Mineral. Geochem. **41**, 35 (2000).

[50] K.S. Kight, Phys. Chem. Miner. **37**, 529 (2010).

[51] A. F. Goncharov, International Journal of Spectroscopy 2012, 617528 (2012), DOI: http://dx.doi.org/10.1155/2012/617528

[52] D. Errandonea, A. Muñoz, P. Rodríguez-Hernández, O. Gomis, S. N. Achary, C. Popescu, S. J. Patwe, and A. K. Tyagi, Inorg. Chem. 55, 4958 (2016).

[53] M. T. Dove, Am. Mineral. 82, 213 (1997).

[54] D. Errandonea, J. Pellicer-Porres, M. C. Pujol, J. J. Carvajal, M. Aguiló, J. Alloys Compd. 638, 14 (2015).

[55] T. Huang, S. R. Shieh, A. Akhmetov, X. Liu, C. M. Lin, and J. S. Lee, Phys. Rev. B 81, 214117 (2010).

[56] P. Botella, R. Lacomba-Perales, D. Errandonea, A. Polian, P. Rodríguez-Hernández, and A. Muñoz, Inorg. Chem. 53, 9729 (2014).

[57] R. Lacomba-Perales, D. Errandonea, D. Martinez-Garcia, P. Rodríguez-Hernández, S. Radescu, A. Mujica, A. Muñoz, J. C. Chervin, and A. Polian, Phys. Rev. B 79, 094105 (2009).

[58] D. Errandonea and F.J. Manjon, Materials Research Bulletin 44, 807 (2009).

[59] O. Gomis, J. A. Sans, R. Lacomba-Perales, D. Errandonea, Y. Meng, J. C. Chervin, and A. Polian, Phys. Rev. B 86, 054121 (2012).

[60] R. Vilaplana, R. Lacomba-Perales, O. Gomis, D. Errandonea, and Y. Meng, Solid State Sciences 36, 16 (2014).

[61] K. Ruschel, L. Nasdala, A. Kronz, J. M. Hanchar, D. M. Többens, R. Škoda, F. Finger, and A. Möller, Miner Petrol 105, 41 (2012).

[62] F. D. Saccone, S. Ferrari, D. Errandonea, F. Grinblat, V. Bilovol, and S. Agouram, J. Appl. Phys. 118, 075903 (2015).

Table I: Structural parameters of the monazite structure ($P2_1/n$) at ambient pressure.

Experiment	a = 7.065(7) Å, b = 7.376(7) Å, c = 6.741(7) Å, β = 103.1(1)º						
Theory	a = 7.0846 Å, b = 7.3843 Å, c = 6.6972 Å, β = 103.27º						
Atom	site	Theory			Experiment		
		x	y	z	x	y	z
Sr	4e	0.2269	0.1574	0.3980	0.22813	0.15869	0.39806
Cr	4e	0.1974	0.1651	0.8860	0.19769	0.16487	0.88691
O_1	4e	0.2583	0.0033	0.0597	0.2584	0.0055	0.0562
O_2	4e	0.1188	0.3393	0.0018	0.1201	0.3373	0.0024
O3	4e	0.0231	0.0256	0.1002	0.1012	0.6917	0.6981
O_4	4e	0.3798	0.3776	0.2214	0.2179	0.7848	0.7881

Table II: Structural parameters of the scheelite structure ($I4_1/a$) at 9.8 GPa (theory) and 9.4 GPa (experiments).

Experiment	a = 4.970(8) Å, c = 11.844(7) Å						
Theory	a = 5.0105 Å, c = 11.8703 Å						
Atom	site	Theory			Experiment		
		x	y	z	x	y	z
Sr	4b	0	0.25	0.625	0	0.25	0.625
Cr	4a	0	0.25	0.125	0	0.25	0.625
O	16f	0.2454	0.1345	0.0471	0.2373(9)	0.1126(9)	0.0451(9)

Table III: Structural parameters of the $AgMnO_4$ structure ($P2_1/n$) at 13.2 GPa (theory) and 13.3 GPa (experiments).

Experiment	a = 6.680(8) Å, b = 6.881(8) Å, c = 6.118(8) Å, β = 92.33(9)°						
Theory	a = 6.6776 Å, b = 6.8970 Å, c = 6.1296 Å, β = 92.63°						
Atom	site	Theory			Experiment		
		x	y	z	x	y	z
Sr	4e	0.3471	0.8639	0.2292	0.3563(1)	0.8743(1)	0.2265(1)
Cr	4e	0.1974	0.6335	0.7727	0.1977(1)	0.6307(1)	0.7620(1)
O_1	4e	0.0052	0.0406	0.2683	0.0200(5)	0.0217(5)	0.2653(5)
O_2	4e	0.1631	0.6127	0.9708	0.1606(5)	0.6140(5)	0.9742(5)
O3	4e	0.2652	0.1541	0.9631	0.2777(5)	0.1591(5)	0.9600(5)
O_4	4e	0.4492	0.8382	0.8232	0.4205(5)	0.8460(5)	0.8212(5)

Table IV: EOS parameters and components of the compressibility tensor of the three differents phases of $SrCrO_4$. These components have been calculated at 0 GPa for the monazite structure, at 8.2 GPa for the scheelite structure, and at 12.4 GPa for the $AgMnO_4$ structure.

	Monazite	Scheelite	$AgMnO_4$
V_0 (Å3)	341(1)	329(1)	327(1)
B_0 (GPa)	59(1)	66(2)	69(3)
B_0'	4.9(5)	4.8(5)	4.5(5)
β_{11} (GPa^{-1})	0.00677	0.00306	0.00263
β_{22} (GPa^{-1})	0.00553	0.00306	0.00256
β_{33} (GPa^{-1})	0.00512	0.00272	0.00279
β_{13} (GPa^{-1})	-0.00225	0	-0.00011

Table V: Ambient pressure experimental and calculated wavenumbers (ω) for Raman modes of monazite-type $SrCrO_4$ (in cm^{-1}) including mode assignment. The pressure coefficients (dω/dP) are also reported (in cm^{-1}/GPa) as well as the Grüneisen parameters (γ). The relative difference between measured and calculated frequencies (R_ω) is also given (in %).

Mode	Theory			Experiments			
	ω	dω/dP	γ	ω	dω/dP	γ	R_ω
B_g	58.4	-0.7	-0.71	----	----	----	----
A_g	64.8	2.2	2.00	67	1.7	1.50	-3.28
A_g	76.6	-2.0	-1.54	78	-0.6	-0.45	-1.79
A_g	91.7	-1.0	-0.64	89	-0.1	-0.07	3.03
B_g	92.2	0.2	0.13	94	0.8	0.50	-1.91
B_g	106.6	1.9	1.05	108	3.2	1.75	-1.30
A_g	109.7	2.2	1.18	----	----	----	----
B_g	114.4	2.0	1.03	114	1.4	0.72	0.35
B_g	119.4	5.0	2.47		----	----	----
A_g	122.7	2.5	1.20	127	4.2	1.95	-3.39
A_g	130.3	3.5	1.58	136	2.3	1.00	-4.19
B_g	155.0	5.1	1.94	144	3.3	1.35	7.64
A_g	158.7	5.3	1.97	161	4.9	1.80	-1.43
B_g	174.7	5.8	1.96	177	----	----	-1.30
B_g	184.4	6.1	1.95	181	----	----	1.88
B_g	192.1	6.3	1.93	187		----	2.73
A_g	192.4	4.9	1.50	196	5.0	1.51	-1.84
A_g	197.4	6.7	2.00	211		----	-6.45
B_g	333.6	0.6	0.11	334	0.6	0.11	-0.12
A_g	344.2	1.8	0.31	342	1.7	0.29	0.64
B_g	349.0	1.3	0.22	350	1.8	0.30	-0.29
A_g	359.9	1.2	0.20	364	1.3	0.21	-1.13
A_g	367.1	2.7	0.43	367	----	----	0.03
B_g	389.4	2.4	0.36	376	2.6	0.41	3.56
A_g	391.8	3.7	0.56	398	3.0	0.44	-1.56
B_g	399.2	2.7	0.40	403	3.3	0.48	-0.94
B_g	423.2	1.9	0.26	424	2.0	0.28	-0.19
A_g	429.1	2.3	0.32	432	2.8	0.38	-0.67
B_g	901.4	4.1	0.27	859	5.3	0.36	4.94
A_g	904.2	4.1	0.27	868	3.9	0.27	4.17
A_g	910.2	4.4	0.29	890	4.9	0.32	2.27
A_g	933.9	5.3	0.33	894	4.8	0.32	4.46
B_g	938.7	4.2	0.26	918	4.4	0.28	2.25
A_g	941.1	4.6	0.29	932	4.7	0.30	0.98
B_g	959.7	4.2	0.26	951			0.91
B_g	975.6	4.3	0.26	970			0.58

Table VI: Experimental and calculated wavenumbers (ω) determined at 8.9 GPa for Raman modes of scheelite-type $SrCrO_4$ (in cm^{-1}) including mode assignment. The pressure coefficients (dω/dP) are also reported (in cm^{-1}/GPa) as well as the experimental Grüneisen parameters (γ). The relative difference between measured and calculated frequencies (R_ω) is also given (in %).

Mode	Theory			Experiments			
	ω	dω/dP	γ	ω	dω/dP	γ	R_ω
E_g	73.6	-3.8	-3.41	72	-2.2	-1.83	2.22
B_g	124.9	0.3	0.16	127	2.9	1.37	-1.65
E_g	164.8	2.7	1.08	162	2.5	0.93	1.73
A_g	175.2	3.2	1.21	----	----	----	----
B_g	219.3	5.8	1.75	221	2.9	0.79	-0.77
E_g	257.5	3.7	0.95	255	5.4	1.27	0.98
B_g	375.1	1.7	0.30	381	2.6	0.41	-1.55
A_g	375.4	2.2	0.39				
B_g	394.4	1.2	0.20	401	3.7	0.55	-1.65
E_g	422.5	1.8	0.28	431	3.3	0.46	-1.97
E_g	932.7	4.9	0.35	888	5.5	0.37	5.03
A_g	936.9	2.9	0.20	898	5.5	0.37	4.33
B_g	988.4	5.5	0.37	953	5.5	0.35	3.71

Table VII: Experimental and calculated wavenumbers (ω) determined at 11.7 GPa for Raman modes of $AgMnO_4$-type $SrCrO_4$ (in cm^{-1}) including mode assignment. The pressure coefficients (dω/dP) are also reported (in cm^{-1}/GPa) as well as the experimental Grüneisen parameters (γ).

Mode	Theory			Experiment		
	ω	dω/dP	γ	ω	dω/dP	γ
B_g	51.6	-3.2	-4.28	70	-0.3	-0.30
A_g	58.9	-0.7	-0.82	78	-0.5	-0.44
A_g	97.2	2.4	1.70	82	0.6	0.50
B_g	98.8	1.4	0.98	94	0.6	0.44
B_g	123.8	2.5	1.39	111	2.0	1.24
A_g	124.1	2.1	1.17	116	1.3	0.77
A_g	143.5	1.2	0.58	126	1.1	0.60
A_g	150.9	2.0	0.91	132	1.5	0.78
B_g	163.9	2.2	0.93	141	1.5	0.73
A_g	164.5	1.9	0.80	154	1.1	0.49
B_g	178.2	2.5	0.97	164	2.9	1.22
A_g	188.1	2.6	0.95	175	4.1	1.62
B_g	218.6	3.7	1.17	187	3.4	1.25
A_g	225.0	4.4	1.35	200	3.8	1.31
B_g	233.2	4.1	1.21	226	3.4	1.04
B_g	237.6	3.6	1.05	235	4.2	1.23
A_g	239.6	3.7	1.07	244	4.2	1.19
B_g	269.7	4.7	1.20	262	2.2	0.58
A_g	342.5	0.8	0.16	----	----	----
B_g	354.5	1.1	0.21	354	1.5	0.29
B_g	372.5	1.1	0.20	371	1.0	0.19
A_g	375.6	2.0	0.37	----	----	----
B_g	378.6	1.6	0.29	387	1.8	0.32
A_g	390.6	2.0	0.35	395	2.8	0.49
B_g	391.0	0.8	0.14	411	1.9	0.32
A_g	430.4	1.7	0.27	419	1.4	0.23
B_g	439.2	2.5	0.39	434	2.2	0.35
A_g	442.7	2.7	0.42	445	3.0	0.47
----	----	----	----	852	2.2	0.18
----	----	----	----	890	2.6	0.20
A_g	926.8	2.5	0.19	904	2.9	0.22
B_g	934.3	2.3	0.17	918	3.7	0.28
A_g	951.6	2.8	0.20	927	3.3	0.25
A_g	964.4	3.1	0.22	933	3.7	0.27
B_g	979.8	3.0	0.21	954	3.2	0.23
B_g	981.6	3.2	0.22	969	2.9	0.21
A_g	997.1	3.5	0.24	996	3.3	0.23
B_g	1041.7	3.6	0.24	1002	3.6	0.25

Figure 1: Enthalpy difference versus pressure taking the monazite structure as reference.

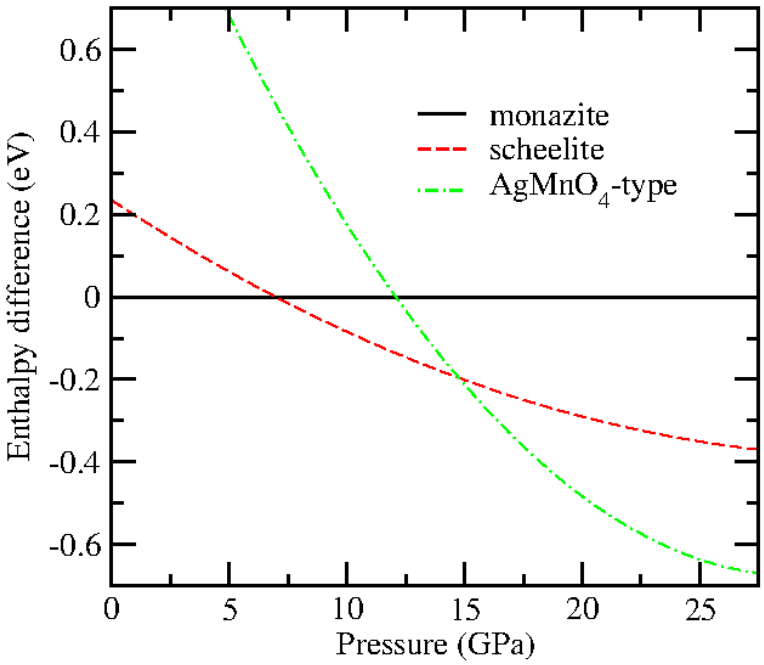

Figure 2: Selection of XRD patterns.

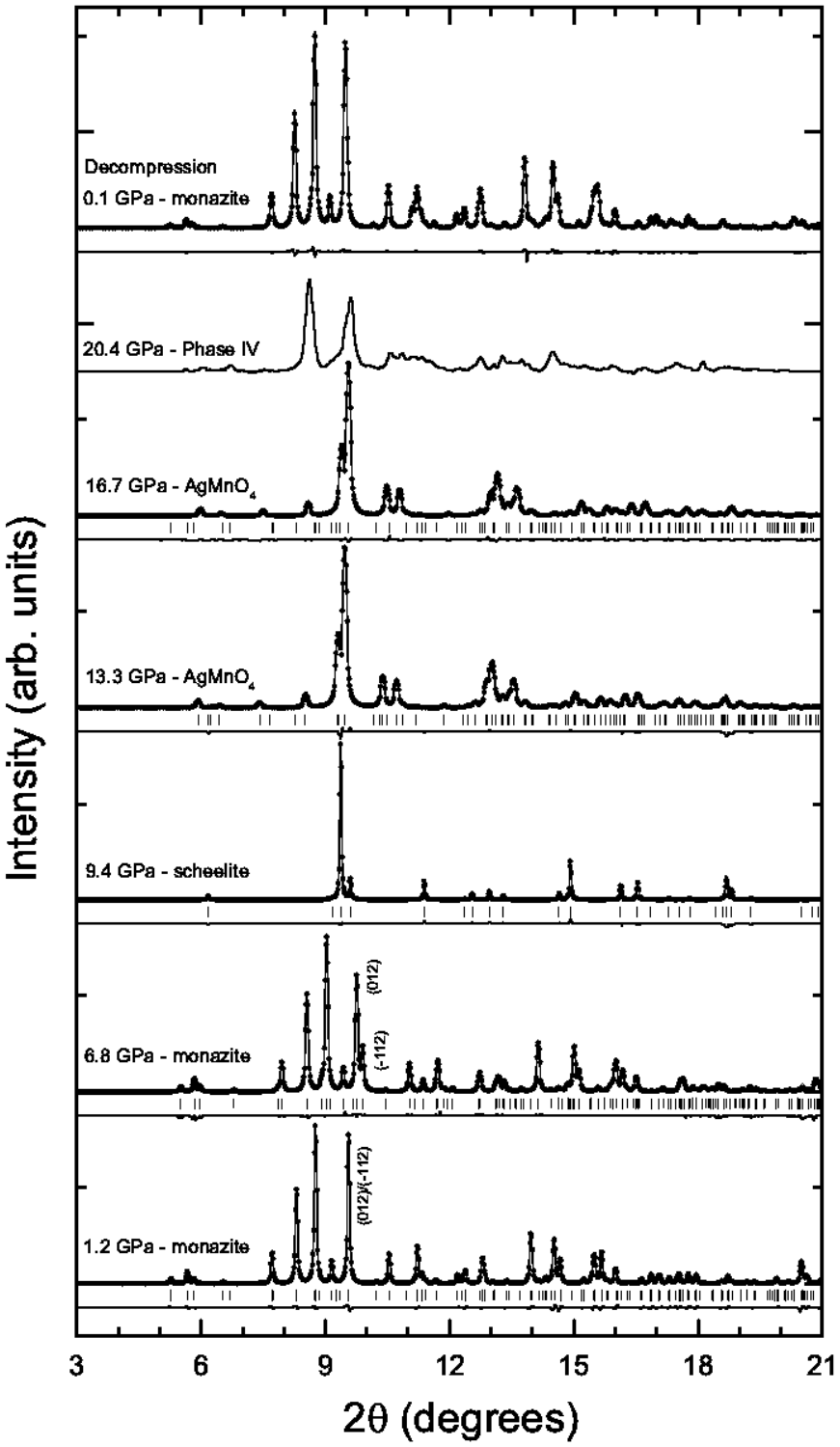

Figure 3: Pressure dependence of the unit-cell parameters and volume.

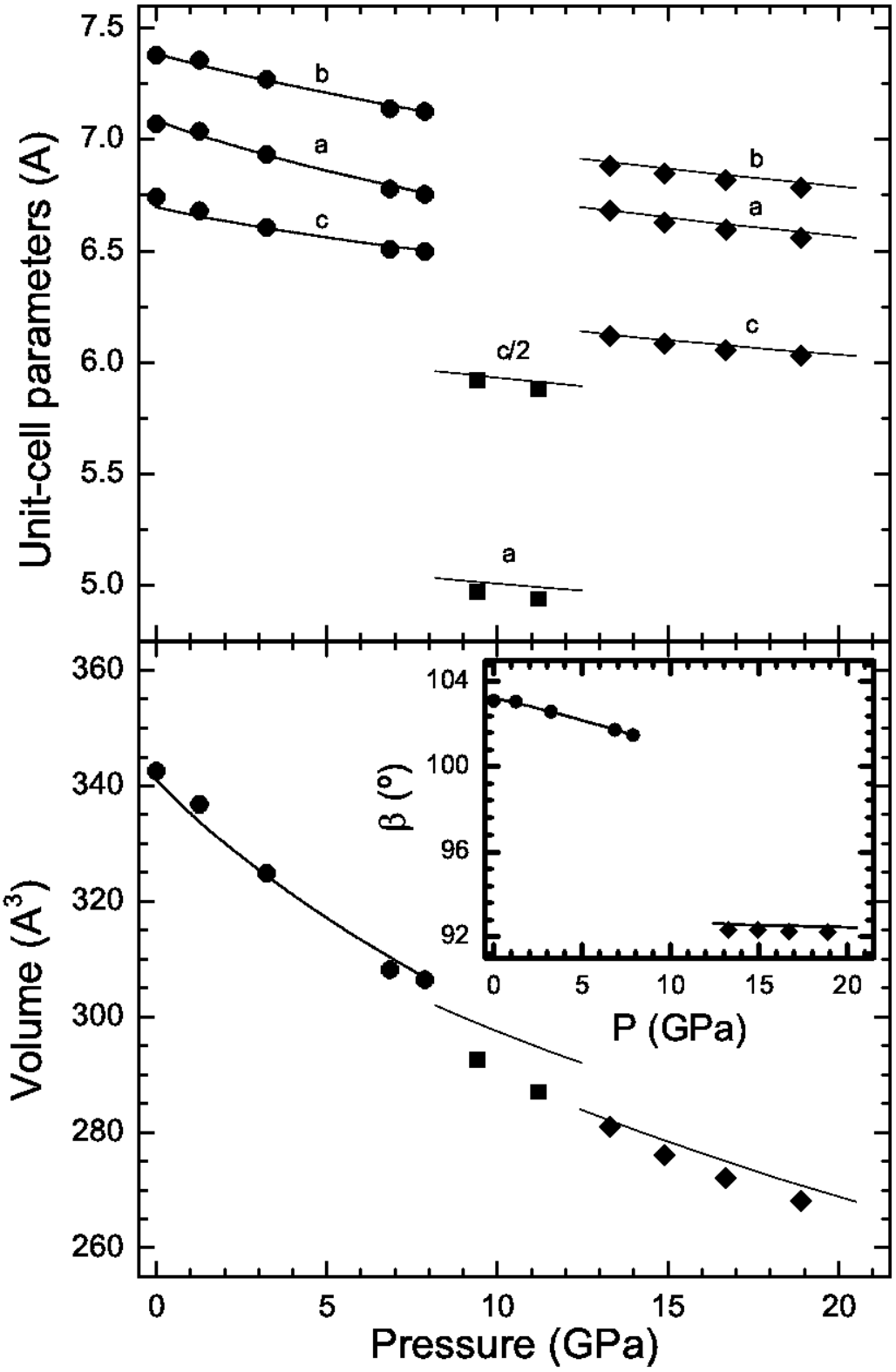

Figure 4: Raman spectra measured at different pressure up to 8.2 GPa using MEW as pressure medium.

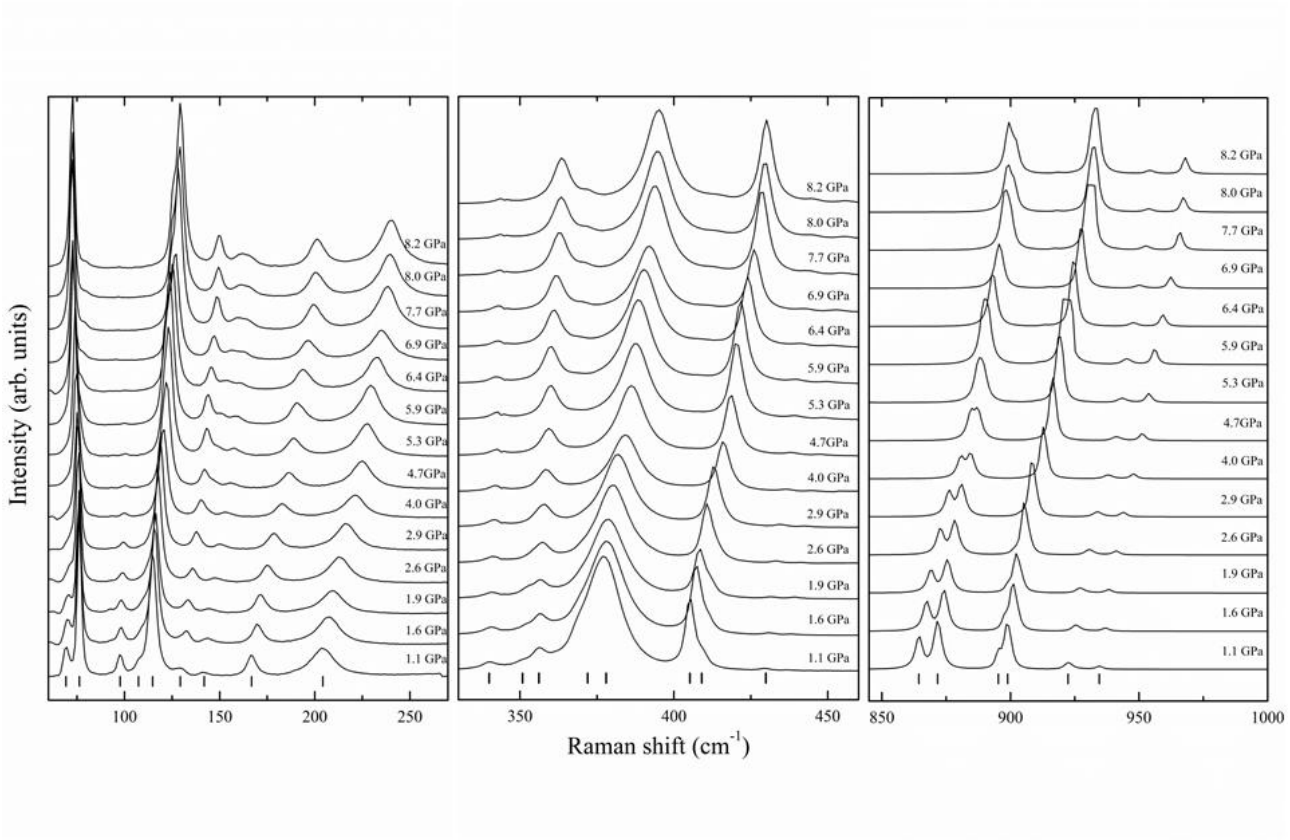

Figure 5: Raman spectra measured at different pressure from 8.2 GPa to 15.7 GPa using MEW as pressure medium.

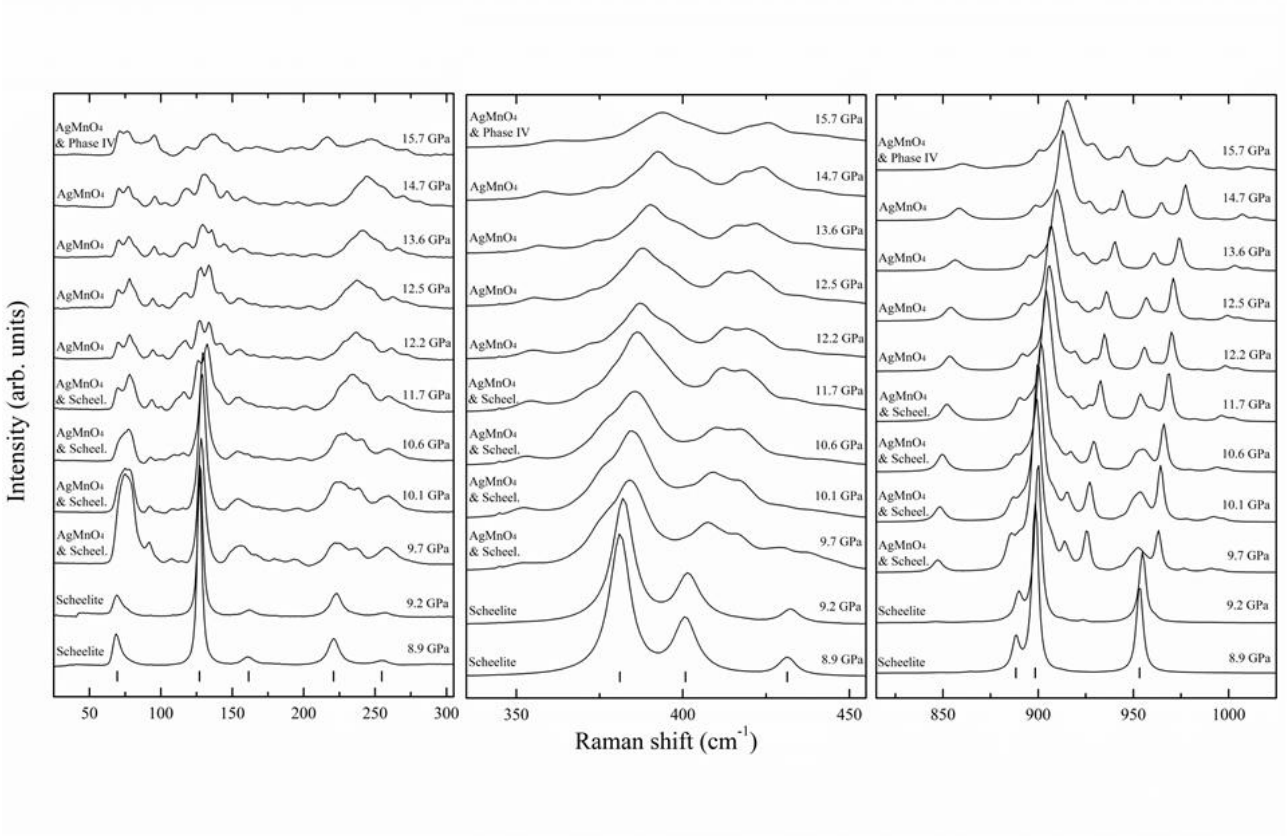

Figure 6: Pressure dependence of the Raman modes of the different phases of $SrCrO_4$.

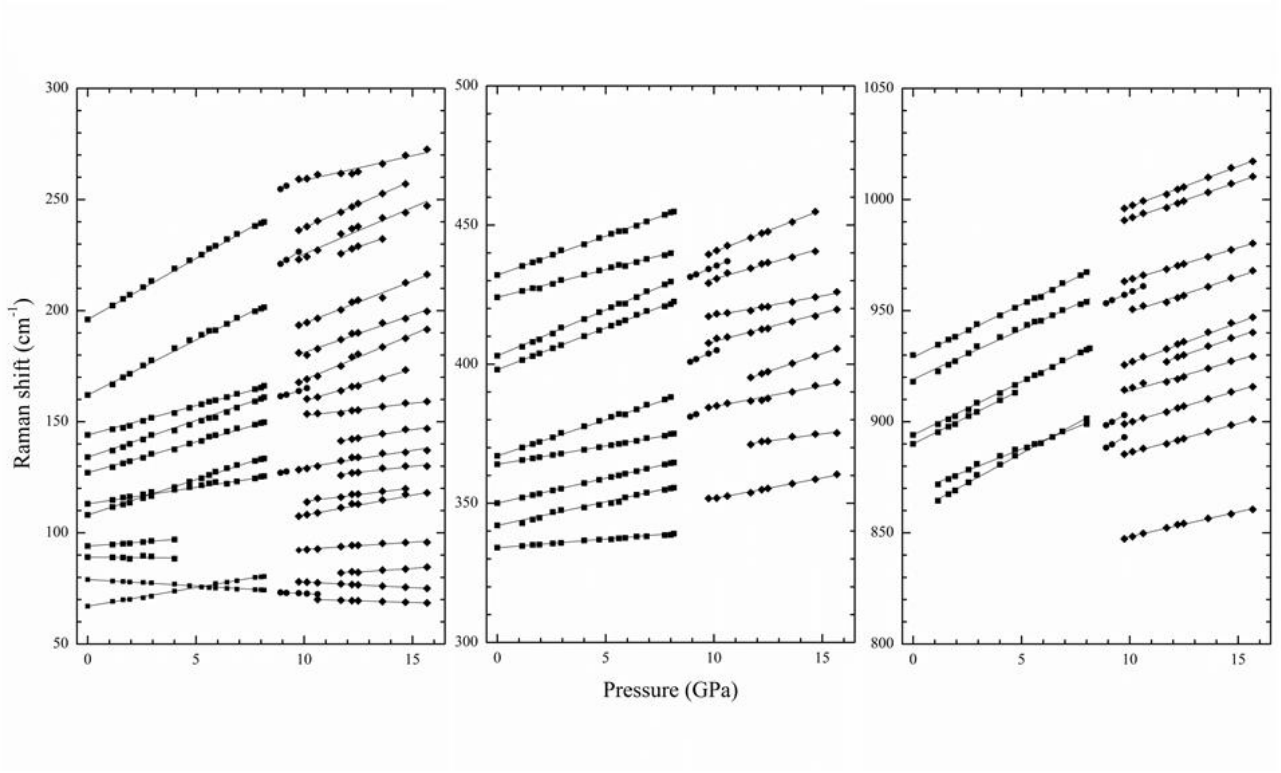

Figure 7: Absorption spectra of $SrCrO_4$ at selected pressures.

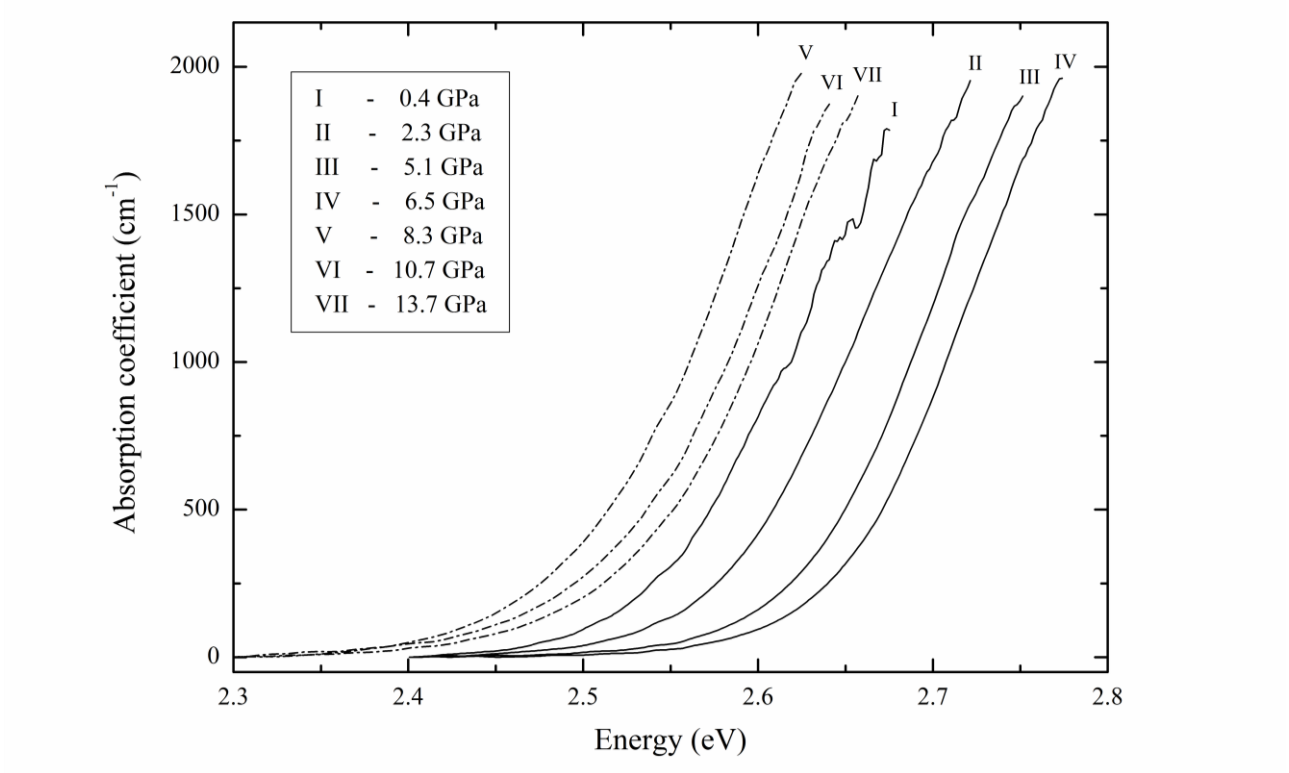

Figure 8: Pressure dependence of the band-gap energy of $SrCrO_4$.